Enhanced sensitivity of mass detection using the first torsional mode of microcantilevers

Hui Xie, Julien Vitard, Sinan Haliyo and Stéphane Régnier

Institut des Systèmes Intelligents et Robotique, Université Pierre et Marie Curie/CNRS,
18 Route du Panorama-BP 61, 92265 Fontenay-aux-Roses, France

E-mail: xie@robot.jussieu.fr

Abstract
Compared with the first flexure mode, higher resonant modes of the microcantilever-based mass sensor promise enhanced sensitivities in bio/chemical mass detection due to higher quality factors. Therefore, the first torsional mode is employed in our research for improved resolution of mass detection. Aiming at accurate characterization of the first torsional mode and further detection of the multi-mass attached to the microcantilevers, a model based on the Rayleigh–Ritz method, considering the attaching positions of the micro/nanoobjects adhered to the microcantilever, is presented. A ragweed pollen, as a target mass, was located at different positions on a commercial microcantilever for the contrasting experiments of the first and second flexures and the first torsional modes of the 'cantilever–object' system in air. Experimental results show that the mass sensitivity of the first torsional mode is an order higher than that of the first bending mode within the realm of existing commercial microcantilevers. The proposed model was further validated by the multi-mass detection results.

Keywords: microcantilever, mass sensors, Rayleigh–Ritz method, ragweed pollen

(Some figures in this article are in colour only in the electronic version)

1. Introduction

Microcantilevers, introduced as nano-probes into the atomic force microscope (AFM) more than two decades ago [1], have been used for a wide variety of applications in bio/chemical detection. One particular kind of application is high-sensitivity mass detection in the dynamic mode by measuring the microcantilevers' resonant frequency shift before and after the load of the additional mass, and is therefore called a cantilever-based mass sensor.

An early application of the cantilever-based mass detection method was the spring constant calibration of the AFM cantilever by measuring its resonant frequency shift due to a known small mass attached to the free end of the cantilever [2]. In contrast with the static method, utilizing the dynamic mode of the microcantilever one can obtain higher sensitivity. Moreover, the cantilever-based mass sensor has abilities to detect various materials in the biological and chemical domains, such as chemical vapors [3], and to detect

molecules [4]. Gradually, the cantilever-based mass sensor has been started to be widely used as a significant scheme for small mass detection. A simple linear electromechanical model of an electrostatic-driven nano-cantilever demonstrated the theoretical sensitivity of the mass detection on the attogram scale [5]. In order to enhance the sensitivity of the mass detection, several cantilevers were fabricated in the nanometer scale using silicon microfabrication technology, which provided promising sensitivity from femtogram to zeptogram [6–12]. The highly sensitive and easily implemented micro/nano-cantilevers were thus widely used in the biological area, including the detection of DNA, virus and cells [13–16]. By measuring the frequency shift and bending of microcantilevers, novel designs for gas and liquid sensing were presented, which can be used to detect mass difference as well as viscosity changes [17, 18]. As an extremely sensitive method, Anderson or vibration localization was used in coupled microcantilevers to detect the mass of a target analyte [19]. In [20], a dynamic method based on the
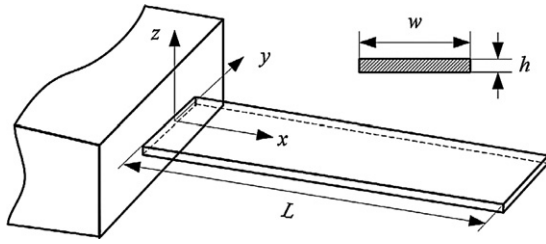
Figure 1. The geometric model of the microcantilever.

Rayleigh–Ritz method was introduced for mass detection and manipulation using the microcantilever. Even the popular nanomaterial—carbon nanotube—was also employed in this hot topic as a nanocantilever toward zeptogram detection [21].

In order to make the cantilever-based mass sensor have ultra-sensitivity within the detection of a single small molecule, besides reducing the feature sizes and increasing the resonant frequencies of the cantilever, higher resonant modes of the cantilever were investigated which have enhanced sensitivities [22, 23]. A resolution of tens of femtogram mass sensing in air was obtained using the second flexural mode of a piezoresistive cantilever [24].

In the AFM application, the first torsional mode of the cantilever has many advantages, in which a noticeable property of torsional resonance is that it is extremely sensitive to the mass at the end of the tip [25]. Therefore, in this paper, motivated by the need for high-sensitivity mass detection of the cantilever-based mass sensor, the first torsional mode is employed to achieve higher sensitivity of mass detection other than the conventional flexural modes. For the modeling of vibration modes of the cantilever, it is found that only a few researchers paid attention to the attaching positions of the micro- and nano-objects. In fact, unless the mass is accurately fabricated on a special position on the cantilever, other mass loading methods such as mass absorbing, accurately placing and distributing will undoubtedly bring positioning errors, in particular directly distributing the mass using micromanipulation, in which adhesion forces play a significant role in physical interactions between micro/nano-objects and the environment or the manipulator [26–28]. Therefore, in this paper, a 'cantilever–object' system model, based on the Rayleigh–Ritz method, considering the attaching position is proposed. In this method, all the dimensions of the microcantilever as well as the attaching position of micro/nano-objects are included in the same model. Once the attaching positions of micro/nano-objects and the first torsional resonant frequency of the cantilever are known, the attaching mass of micro/nano-objects can be precisely determined.

2. Theories and models

2.1. Model of the cantilever

As shown in figure 1, a microcantilever with a rectangular section is fixed at one end and free at the other end, assumed to deform in a linear elastic range. Dimensions L, w and h are the length, width and thickness of the microcantilever, respectively. The coordinates are defined as follows: the origin is located at the center of the cross section of the built-in end, the x-axis is along its length, and the z-axis and y-axis are along its thickness and width, respectively. The motion of the torsional modes of the microcantilever is a function of x [29]:

$$GJ\frac{\partial^2\theta(x,t)}{\partial x^2} = \rho I_p\frac{\partial^2\theta(x,t)}{\partial t^2} + c\frac{\partial\theta(x,t)}{\partial t}, \qquad (1)$$

where $\theta(x,t)$ is the rotation angle of the cantilever along its x-axis, G is the shear modulus, ρ is the density of the cantilever, c is the coefficient of viscous damping, the polar area moment of inertia $I_p = (wh^3 + w^3h)/12$ and J is the torsional constant. For the rectangular cantilever, J can be obtained by [30]

$$J \approx \frac{1}{3}wh^3\left[1 - 0.63\frac{h}{w} + 0.052\left(\frac{h}{w}\right)^5\right], \qquad (2)$$

The nth torsional resonant frequency is obtained by

$$\omega = \frac{(2n-1)\pi}{2L}\sqrt{\frac{GJ}{\rho I_p}}, \qquad n = 1, 2, \ldots. \qquad (3)$$

2.2. The Rayleigh–Ritz method

Hundreds of papers have been published that used a method, termed the 'Rayleigh–Ritz method', to resolve natural frequencies of continuum systems. Although it was claimed that Rayleigh's name should not be attached to the Ritz method, that is, the 'Rayleigh–Ritz method' is an improper designation [31], the classic and perfect method will be employed to solve the natural frequencies of the cantilever–mass system in our research. In the Rayleigh method, the potential (U) and kinetic (T) energies of the torsional system are considered to calculate the natural frequency of the system. The maxima $U_{\max}$ and $T_{\max}$ are defined by

$$U_{\max} = \frac{1}{2}\int_0^L GJ\left[\frac{\partial z(x)}{\partial x}\right]^2 dx \qquad (4)$$

$$T_{\max} = \frac{1}{2}\omega^2\int_0^L \rho I_p z^2(x)\, dx, \qquad (5)$$

where $z(x)$ is the mode shape of the cantilever. In this method, by assuming the function of the mode shape $z(x)$ and setting the maximum potential energy $U_{\max}$ and kinetic energy $T_{\max}$ in a cycle of vibration equal to each other, the natural frequency ω of a continuum system can be determined by

$$\omega^2 = \frac{\int_0^L GJ\left[\frac{\partial z(x)}{\partial x}\right]^2 dx}{\int_0^L \rho I_P z^2(x)\, dx}. \qquad (6)$$

Obviously, the calculation accuracy of the resonant frequency has a strong dependence on the accuracy of the assumed function, i.e. how closely the assumed mode shape fits the exact one, especially for a system with multi-subsystems. In Ritz's method, a displacement function on x is assumed in terms of a series of displacement functions with undetermined coefficients that meet the geometric boundary conditions of the vibration. Thus, the mode function is defined by

$$v(x) = \sum_{i=0}^n a_i\varphi_i(x), \qquad (7)$$
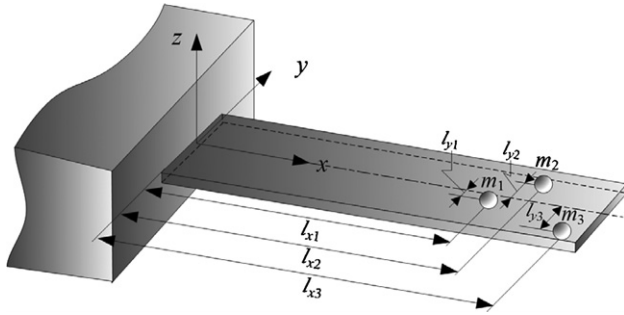
Figure 2. The geometric model of the 'cantilever–object' system. Three microspheres m_1, m_2 and m_3 attached to the cantilever have coordinates of (l_{x1}, l_{y1}), (l_{x2}, l_{y2}) and (l_{x3}, l_{y3}), respectively.

where the shape function $\phi_i(x)$ may be defined as polynomials or trigonometric functions and a_i are arbitrary coefficients.

From (6) and (7), a similar equation for the natural frequency can be given by

$$\omega^2 = \frac{\{a\}^T[K]\{a\}}{\{a\}^T[M]\{a\}} = \frac{K}{M}, \tag{8}$$

where $\{a\}^T = \{a_1, a_2, \ldots, a_n\}$, K and M are stiffness and mass matrices, respectively. According to (8), the solution of the natural frequency is given by

$$[K - \omega^2 M]\{a\} = 0. \tag{9}$$

Therefore, for the arbitrary coefficients $\{a\}$, the solution is

$$\det(K - \omega^2 M) = 0. \tag{10}$$

This is the famous Rayleigh–Ritz method for the calculation of the natural frequency of the continuum systems. For a complex system consisting of multi-subsystems, for example if a spring bearing or mass adhered to the vibrating continuum systems, their additional potential or kinetic energies should be added to the whole system. Therefore, in the 'cantilever–mass' system, after adding the kinetic energy of the mass to the whole system, the natural frequency of the whole system can be accurately calculated.

2.3. Analysis of the torsional vibration

The 'cantilever–object' system is modeled in figure 2. The torsional axis is along the x-axis and through the center of the cross section of the built-in end. In the model of the first torsional mode, three micro-objects, assumed to have the same mass m, attached to locations (l_{xk}, l_{yk}), and two degrees of freedom t_1 and t_2 that are vertical to the x-axis, are assigned to the whole system. Thus, the shape function of the first torsional mode can be defined as

$$z_t(x) = t_1\psi_1(x) + t_2\psi_2(x), \tag{11}$$

where the functions $\psi_1(x)$ and $\psi_2(x)$, presenting the torsional angle of the cantilever, are defined as x and x^2, respectively. t_1 and t_2 are two corresponding coefficients. Therefore, the maximum potential (U_{max}) and maximum kinetic (T_{max}) energies of the beam in the first torsional mode are given by

$$U_{max} = \frac{1}{2}GJ \int_0^L \left[\sum_{i=1}^2 t_i \frac{\partial \psi_i(x)}{\partial x} \right] \left[\sum_{j=1}^2 t_j \frac{\partial \psi_j(x)}{\partial x} \right] dx \tag{12}$$

$$T_{max} = \frac{1}{2}\rho I_p \omega^2 \int_0^L \left[\sum_{i=1}^2 t_i \psi_i(x) \right] \left[\sum_{j=1}^2 t_j \psi_j(x) \right] dx. \tag{13}$$

Thus, the factors of the matrices K and M for the torsional mode are obtained by

$$k_{ij} = GJ \int_0^L \frac{\partial \psi_i(x)}{\partial x} \cdot \frac{\partial \psi_j(x)}{\partial x} dx \tag{14}$$

$$m_{ij} = \rho I_p \int_0^L \psi_i(x) \cdot \psi_j(x) dx. \tag{15}$$

For the attaching objects, the corresponding elements of the mass matrix are given by

$$m_{ij\,object} = \sum_{n=1}^3 J_{mk}\psi_i(x) \cdot \psi_j(x), \tag{16}$$

where k is the number of the three micro/nano-objects and J_m is the inertia moment of mass. For a microsphere, J_m can be given by

$$J_m = \frac{2}{5}mr^2 + m\left[l_{yk}^2 + \left(\frac{h}{2} + r \right)^2 \right], \tag{17}$$

where r is the radius of the attaching microsphere. Therefore, under the given coordinate system and $[t_1, t_2]$, the mass matrix M and the stiffness matrix K of the whole system are determined as

$$M = \begin{bmatrix} \frac{1}{3}\rho I_P L^3 + \sum_{k=1}^3 J_{mn}l_{xn}^2 & \frac{1}{4}\rho I_p L^4 + \sum_{k=1}^3 J_{mn}l_{xn}^3 \\ \frac{1}{4}\rho I_p L^4 + \sum_{k=1}^3 J_{mn}l_{xn}^3 & \frac{1}{5}\rho I_p L^5 + \sum_{k=1}^3 J_{mn}l_{xn}^4 \end{bmatrix} \tag{18}$$

$$K = \begin{bmatrix} GJL & GJL^2 \\ GJL^2 & \frac{4}{3}GJL^3 \end{bmatrix}. \tag{19}$$

From (10), a solution involves parameters of inertia moment J_{mk}; the natural resonant frequency ω of the 'cantilever–object' system is obtained by

$$f(l_{xk}, J_{mk}, \omega) = 0 \qquad (k = 1, 2, \ldots, N). \tag{20}$$

Note that in (20), there are three variables. l_{xk} is the longitude position of microspheres, and the inertia moment of mass J_{mk} is determined by the mass and the position of the object from the torsional axis. Therefore, if we know the resonant frequency of the 'cantilever–object' system and the attaching positions of microspheres, the mass can be calculated.

3. Experiments and results

3.1. Set-up of the cantilever-based mass sensor

The mass sensor used in our experiments mainly consists of a silicon microcantilever, a piezoceramic and a laser deflection measuring system. The piezoceramic, as a vibration actuator,

has dimensions of 1 mm in thickness, 5 mm in width and 8 mm in length. Experimental results indicate that this piezoceramic has a linear relation between voltage input and displacement output, from 0 to 60 nm under the input between 0 and 300 V. A signal generator is used to actuate the piezoceramic, which can produce asinusoidal waves ranging from 0 to 20 V, with the bandwidth ranging from 1 to 3 MHz and resolutions of 1 Hz from 0 to 10 kHz, 10 Hz below 1 MHz, 100 Hz within the range of 1–3 MHz. An optical microscope (Olympus BX50WI with 20× objective, providing a resolution of 0.55 μm pixel^{-1}) is employed to measure the attaching positions of the micro/nano-objects and to determine the dimensions of the cantilever.

3.2. Calibration of the cantilever

The spring constant of microcantilevers should be accurately determined. Many methods, including dynamic methods (forced and thermal oscillation), static loading and FEA methods, were used to calibrate the stiffness of the cantilever [32]. During the calibration, although dimensions of the cantilever were provided by the manufacturer, the optical microscope was used to measure the cantilever's dimensions. In our experiment, the forced oscillation method was employed to determine the key parameter h of the cantilever based on its natural frequency.

As shown in figure 3(a), the experimental cantilever has a wedge-shaped end. Therefore, considering the effect of the wedge-shaped end of the cantilever, (14) and (15) should be modified for the first torsional model:

$$k_{ij} = GJ \int_0^{L-l_w} \frac{\partial^2 \psi_i(x)}{\partial x^2} \cdot \frac{\partial^2 \psi_j(x)}{\partial x^2}\, dx$$
$$+ GJ \int_{L-l_w}^L \frac{(L-x)}{l_w} \cdot \frac{\partial^2 \psi_i(x)}{\partial x^2} \cdot \frac{\partial^2 \psi_j(x)}{\partial x^2}\, dx \qquad (21)$$

$$m_{ij} = \rho I_p \int_0^{L-l_w} \psi_i(x) \cdot \psi_j(x)\, dx$$
$$+ \rho I_p \int_{L-l_w}^L \frac{(L-x)}{l_w} \cdot \psi_i(x) \cdot \psi_j(x)\, dx, \qquad (22)$$

where l_w is the height of the wedge tip on the x-axis. If the first torsional frequency of the cantilever is known, the thickness of the cantilever can be calculated by the modified (20) (set $J_m = 0$). In the experiments, dimensions of the cantilever were measured as 596.5 μm in length, 141.5 μm in width and $l_w = 68.4$ μm under the optical microscope. Finally, the spring constant was characterized as 20.15 N m^{-1}.

3.3. Mass sensitivity of the first three modes

The resonant frequencies of the microcantilever were detected by a laser deflection measuring system, which mainly consists of a laser, a quadrant photodiode and some other components to build the light path. Each of the first three modes was examined separately. Indeed, it is possible to carefully locate the laser spot at the center of the free end of the microcantilever to maximize the contribution of the torsional mode [33]. After carefully preparing the experimental system, the first step
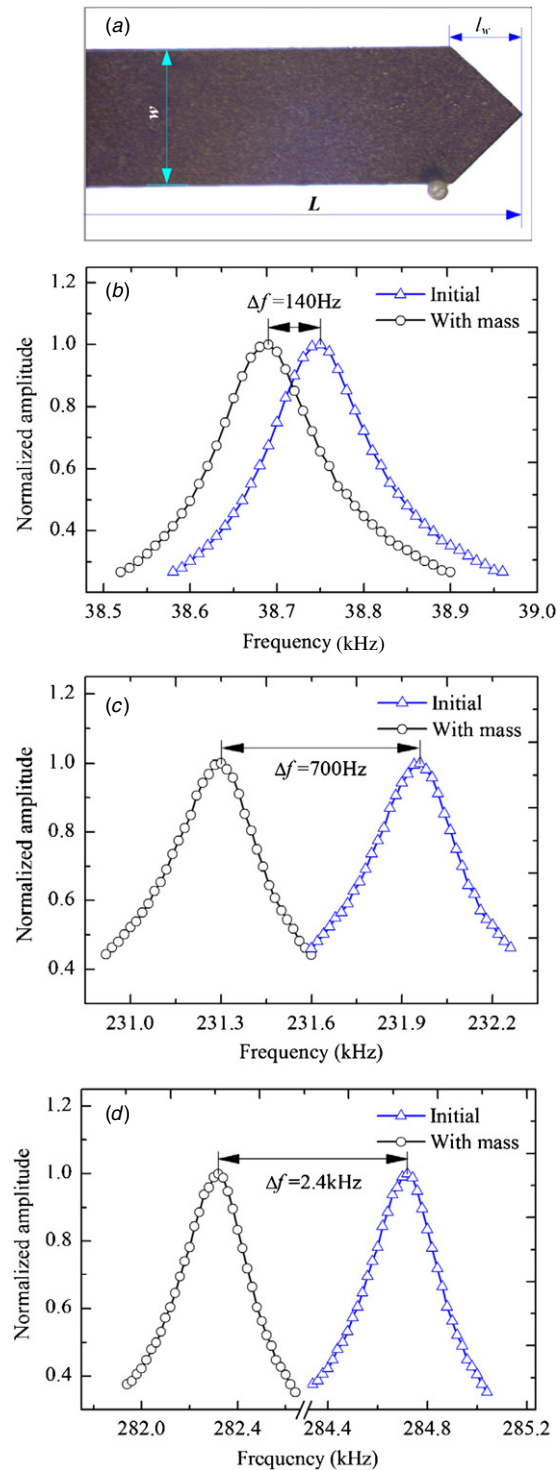
Figure 3. (a) An optical image of the microcantilever with an attached ragweed pollen. (b) Frequency shift of the first flexural mode. (c) Frequency shift of the second flexural mode. (d) Frequency shift of the first torsional mode.

was to characterize the natural frequencies of the cantilever by performing a frequency sweep from 0 to 300 kHz with an interval of 10 Hz; then a grain of ragweed pollen with a diameter of 20–20.5 μm was released on the free end of

Table 1. Mass detection results using the first three modes.

Descriptions	1st flexural	2nd flexural	1st torsional	Average
Mass (10^{-12} kg)	3.795	3.879	3.848	3.841

Table 2. The mass detection of the ragweed pollen adhered to the cantilever at different positions.

Sequences	Positions (x, y) (μm)	1st torsional freq. shift (kHz)	Gross mass (10^{-12} kg)
1	(491, 68)	1.81	3.829
2	(536, 17)	0.12	2.984
3	(530, −38)	0.61	3.816
4	(519, −77)	2.40	3.848

the microcantilever (shown in figure 3(*a*)). In order to get high sensitivity of the mass detection, the ragweed pollen was purposefully located near the edge of the microcantilever on the free end. Under an optical microscope, the position of the ragweed pollen was measured as (519, −77) (μm) in the given coordinate as shown in figure 2. When the ragweed pollen was placed, the experiment was rerun to determine the first three resonant frequencies of the 'cantilever–object' system. During the sweeping, the first three resonant frequencies without and with this added mass were recorded. In figures 3(*b*)–(*d*), we can get that the frequency shifts of these first three modes are 140 Hz, 700 Hz and 2.4 kHz, respectively, which indicate that the first torsional mode has relatively the highest sensitivity of mass detection. The second flexural mode also has a high sensitivity due to the smaller effective mass of the microcantilever than the first bending mode [24]. As shown in table 2, using these three modes, an average mass of the ragweed pollen was measured as 3.838 × 10^{-12} kg under a humidity of 60%, which is quite in accordance with the previous experimental result [34].

In the experiments, the natural frequency of the 'cantilever–object' system was measured using a sinusoidal excitation with a very low magnitude to guarantee the weak adhesion force between the cantilever and the ragweed pollen to be enough to hold the ragweed pollen in such high frequency (the first torsional resonant frequency of the cantilever is 284.72 kHz). The experimental results show that the first torsional resonant frequency of the system strongly depends on the attaching position of the microsphere. In order to validate the relationship among the resonant frequencies, attaching positions and mass of the microsphere, as shown in figure 4, the ragweed pollen was located at four different positions along the *y*-axis. From (20), because the natural frequency is determined by the positions on the *x*- and *y*-axes as well as the mass of the ragweed pollen, this problem is resolved as follows. Initially, the microscopic vision was employed to measure the attaching position of the ragweed pollen. Secondly, the first torsional resonant frequency of the 'cantilever–object' system was detected by the frequency sweep. Subsequently, the mass of the ragweed pollen was easily calculated from (20). The corresponding experimental results are shown in table 2. Note that the frequency shift, related to the detection sensitivity
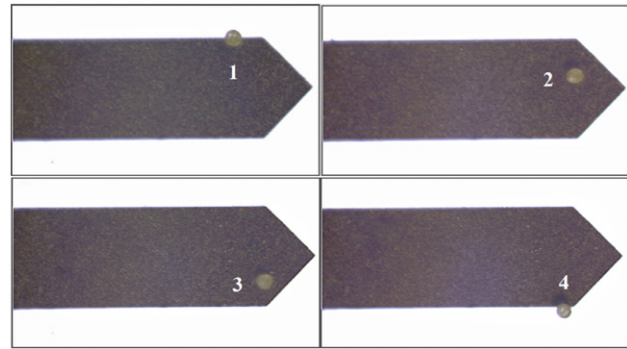
Figure 4. The ragweed pollen is placed at four different positions along the transversal coordinate of the microcantilever.
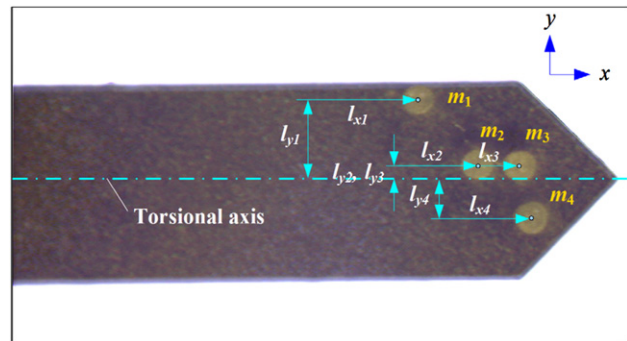
Figure 5. Four ragweed pollens adhered to the cantilever at different positions. The positions are measured by microscopic vision with a resolution of 0.55 μm pixel^{-1}.

Table 3. Results of the multi-mass detection.

Ragweed pollens	Positions (l_{xk}, l_{yk}) (μm)	1st torsional freq. shift (kHz)	Mass (10^{-12} kg)
1	(461, 55)	1.82	3.905
2	(509, 10)		
3	(532, 10)		
4	(540, −28)		

of the mass detection, will be decreased when the attaching position of the ragweed pollen approaches the torsional axis of the microcantilever due to its decreasing moment of inertia, which is in accordance with the analysis of the torsional mode of the cantilever-based mass sensor. Therefore, in order to get high sensitivity of the mass detection in the first torsional mode, the mass should be placed near the edge of the cantilever.

3.4. Multi-mass detection

In order to further verify the proposed mode, as shown in figure 5, four ragweed pollens were released on the free end of the cantilever with different positions that were measured under the optical microscope. As shown in table 3, an average mass 3.905 × 10^{-12} kg was detected by the proposed method, which is a little higher than the real mass of the ragweed pollen. Two factors contribute to this error; the first one is that the diameter difference of the ragweed pollen results in errors

in the mass detection, and the other is that two ragweed pollens m_2 and m_3 are near the torsional axis of the microcantilever, reducing the sensitivity of the mass detection. However, in contrast with the conventional flexural mode, the first torsional mode has much higher mass sensitivity when the mass is placed near the edge of the free end of the microcantilever, which promises the possibility of using ordinary microcantilevers for higher sensitivity in bio/chemical detection.

4. Conclusion

In order to achieve higher sensitivity mass detection, a model for the first torsional mode of the 'cantilever–object' system based on the Rayleigh–Ritz theory was developed. A ragweed pollen was released on the edge of the free end of the microcantilever to purposefully compare the mass sensitivities of the first three modes of the microcantilever. The experimental results show that the mass sensitivity of the first torsional mode is an order of magnitude greater than the first flexure mode, and much higher than that of the second resonant mode. In order to verify the effect of positions on the sensitivity of the first torsional mode, the ragweed pollen was deliberately placed at four different positions on the transverse axis near the cantilever free end and the positions were measured by highly precise microscopic vision. The experimental results indicated that when the ragweed pollen nears the edge of the cantilever, higher sensitivity of mass detection could be achieved. In the multi-mass detection, four ragweed pollens were released on the cantilever and the mass was also accurately detected. In conclusion, using the first torsional resonant mode of the microcantilever, one can achieve enhanced mass sensitivity with commercial microcantilevers.

References

[1] Binning G, Quate C F and Gerber C 1986 Atomic force microscope *Phys. Rev. Lett.* **56** 930–3

[2] Cleveland J P and Manne S 1993 A nondestructive method for determining the spring constant of cantilevers for scanning force microscopy *Rev. Sci. Instrum.* **64** 403–5

[3] Thundat T, Wachter E A, Sharp S L and Warmack R J 1995 Detection of mercury-vapor using resonating microcantilevers *Appl. Phys. Lett.* **66** 1695–7

[4] Ono T, Li X X, Miyashita H and Esashi M 2003 Mass sensing of adsorbed molecules in sub-picogram sample with ultrathin silicon resonator *Rev. Sci. Instrum.* **74** 1240–3

[5] Abadal G, Davis Z J, Helbo B, Borrise X, Ruiz R, Boisen A, Campabadal F, Esteve J, Figueras E, Perez-Murano F and Barniol N 2001 Electromechanical model of a resonating nano-cantilever-based sensor for high-resolution and high-sensitivity mass detection *Nanotechnology* **12** 100–4

[6] Davis Z J, Abadal G, Kuhn O, Hansen O, Grey F and Boisen A 2000 Fabrication and characterization of nanoresonating devices for mass detection *J. Vac. Sci. Technol.* **18** 612–6

[7] Lavrik V N and Datskos P G 2003 Femtogram mass detection using photothermally actuated nanomechanical resonators *Appl. Phys. Lett.* **82** 2697–9

[8] Ilica B, Craighead H G, Krylov S, Senaratne W, Ober C and Neuzil P 2004 Attogram detection using nanoelectromechanical oscillators *J. Appl. Phys.* **95** 3694–703

[9] Arlett J L, Maloney J R, Gudlewski B, Muluneh M and Roukes M L 2006 Self-sensing micro- and nanocantilevers with attonewton-scale force resolution *Nano Lett.* **6** 1000–6

[10] Hosaka S, Chiyoma T, Ikeuchi A, Okano H, Sone H and Izumi T 2006 Possibility of a femtogram mass biosensor using a self-sensing cantilever *Curr. Appl. Phys.* **6** 384–8

[11] Shen Z Y, Shih W Y and Shih W H 2006 Self-exciting, self-sensing PbZr$_{0.53}$Ti$_{0.47}$O$_3$/SiO$_2$ piezoelectric microcantilevers with femtogram/Hertz sensitivity *Appl. Phys. Lett.* **89** 023506

[12] Yang Y T, Callegari C, Feng X L, Ekinci K L and Roukes M L 2006 Zeptogram-scale nanomechanical mass sensing *Nano Lett.* **6** 583–6

[13] Su M, Li S Y and Dravid V P 2003 Microcantilever resonance-based DNA detection with nanoparticle probes *Appl. Phys. Lett.* **82** 3562–4

[14] Ilic B, Czaplewski D, Zalalutdinov M and Craighead H G 2001 Single cell detection with micromechanical oscillators *J. Vac. Sci. Technol.* B **19** 2825–8

[15] Gupta A, Akin D and Bashir R 2003 Single virus particle mass detection using microresonators with nanoscale thickness *Appl. Phys. Lett.* **84** 1976–8

[16] Gupta A and Akin D 2004 Detection of bacterial cells and antibodies using surface micromachined thin silicon cantilever resonators *J. Vac. Sci. Technol.* B **22** 2785–91

[17] Vidic A, Then D and Ziegler C H 2003 A new cantilever system for gas and liquid sensing *Ultramicroscopy* **97** 407–16

[18] Hagleitner C, Hierlemann A, Lange D, Kummer A, Kerness N, Brand O and Baltes H 2001 Smart single-chip gas sensor microsystem *Nature* **414** 293–6

[19] Spletzer M, Raman A, Wu A Q and Xu X F 2006 Ultrasensitive mass sensing using mode localization in coupled microcantilevers *Appl. Phys. Lett.* **88** 254102

[20] Haliyo S, Régnier S and Guinot J C 2003 [*mü*]MAD, the adhesion based dynamic micromanipulator *Eur. J. Mech.* **22** 903–16

[21] Nishio M, Sawaya S, Akita S and Nakayama Y 2005 Carbon nanotube oscillators toward zeptogram detection *Appl. Phys. Lett.* **86** 133111

[22] Sharos L B, Raman A, Crittenden S and Reifenberger R 2004 Enhanced mass sensing using torsional and lateral resonances in microcantilevers *Appl. Phys. Lett.* **84** 4638–40

[23] Dohn S, Sandberg R, Svendsen W and Boisen A 2005 Enhanced functionality of cantilever based mass sensors using higher modes *Appl. Phys. Lett.* **85** 233501

[24] Jin D Z, Li X X, Liu J, Zuo G M, Wang Y L, Liu M and Yu H T 2006 High-mode resonant piezoresistive cantilever sensors for tens-femtogram resoluble mass sensing in air *J. Micromech. Microeng.* **16** 1017–23

[25] Bhushan B, Fuchs H and Kawata S 2007 *Applied Scanning Probe Methods V: Scanning Probe Microscopy Techniques* (Berlin: Springer)

[26] Rollot Y, Régnier S and Guinot J C 1999 Simulation of micro-manipulations: adhesion forces and specific dynamic models *Int. J. Adhes. Adhes* **19** 35–48

[27] Rollot Y, Régnier S and Guinot J C 2002 Dynamical model for the micro-manipulation by adhesion: experimental validations for determined conditions *J. Micromechatron.* **1** 273–97

[28] Lambert P and Régnier S 2006 Surface and contact forces models within the framework of microassembly *J. Micromechatron.* **3** 123–57

[29] Gorman D J 1975 *Free Vibration Analysis of Beams and Shafts* (New York: Wiley)

[30] Ross C T F 1991 *Finite Element Programs for Structural Vibrations* (London: Springer)

[31] Leissa A W 2005 The historical bases of the Rayleigh and Ritz methods *J. Sound Vib.* **287** 961–78

[32] Burnham N A, Chen X, Hodges C S, Matei G A, Thoreson E J, Roberts C J, Davies M C and Tendler S J B 2003 Comparison of calibration methods for atomic force microscopy cantilevers *Nanotechnology* **14** 1–6

[33] Cannara R J, Eglin M and Carpick R W 2006 Lateral force calibration in atomic force microscopy: a new lateral force calibration method and general guidelines for optimization *Rev. Sci. Instrum.* **77** 053701

[34] Harrington J B Jr and Metzger K 1963 Ragweed pollen density *Am. J. Botany* **50** 532–9